Self-Organization Kinetics of Mesoporous Nanostructured Particles

Leon Gradoń
Dept. of Chemical Engineering, Warsaw University of Technology, 00-645 Warsaw, Poland

Stanislaw Janeczko
Dept. of Mathematics and Information Sciences, Warsaw University of Technology, 00-661 Warsaw, Poland

Mikrajuddin Abdullah, Ferry Iskandar, and Kikuo Okuyama
Dept. of Chemical Engineering, Graduate School of Engineering, Hiroshima University, Higashi Hiroshima 739-8527, Japan

DOI 10.1002/aic.10257
Published online in Wiley InterScience (www.interscience.wiley.com).

Spray drying a mixture of silica and polystyrene latex (PSL) colloids above the decomposition temperature of PSL results in the formation of porous silica particles. By appropriate selection of the experimental conditions, such as the use of a tubular temperature, the weight fraction of colloids, and the flow rate of carrier gas, the resulting silica particles contain organized pores with a hexagonal close-packing arrangement. The process by which organized mesoporous silica particles are formed by the spray-drying method was examined using elementary laws of topology. Although a direct test using experimental data was not performed, at least qualitatively, the existence of a "stationary state" at which organized mesoporous particles can be produced with hexagonal close packing could be defined. Deviation from this stationary state results in the formation of unorganized pores as well as a deformed particle shape, rather than spherical ones. © 2004 American Institute of Chemical Engineers *AIChE J,* 50: 2583–2593, 2004
Keywords: mesoporous particles, nanostructure, polystyrene latex, topology, stationary state

Introduction

Catalysis, chromatography, the controlled release of drugs, low dielectric constant fillers, sensors, pigments, microelectronics, and electro-optics all represent examples of applications of mesoporous materials (see Huo et al., 1997; Ozin, 1992; Velev et al., 1997). Such materials are frequently prepared using a colloidal crystal template on a plate substrate (see Park et al., 1998; Velev and Kaler, 2000; Velev et al., 1997; Zakhidov et al., 1998). The procedure typically consists of three main steps: (1) the formation of colloidal crystals; (2) infiltration of the voids between the colloidal beads with other materials [a second colloid, or reactant gases in the case of a chemical vapor deposition (CVD) reactor, or reactant ions in the case of an electrochemical cell]; and (3) the removal of the colloidal beads chemically or thermally, leaving behind a porous material that is an inverse replica of the mesostructure of the template. This, however, requires numerous processing steps and is time consuming. The entire process requires several hours or longer for completion. We recently reported on an aerosol-assisted spray-drying method for producing powder particles, in an organized mesoporous state. As shown by Iskandar et al. (2001a, 2002), this procedure requires only several seconds to reach completion.

Both the controllability of the pore size and the morphology

Permanent address of M. Abdullah: Dept. of Physics, Bandung Institute of Technology, Jalan Ganeca 10, Bandung 40132, Indonesia.
Correspondence concerning this article should be addressed to K. Okuyama at okuyama@hiroshima-u.ac.jp.

of the final product are important for the development of size-selective filters and a selective optical cavity (see, for example, Iskandar et al., 2003a,b). The wavelength of the optical mode in a cavity is dependent on the cavity size and the band gap of the optical crystals is dependent on the crystal periodicity. Here, we report on the preparation of organized mesoporous silica particles, in which the pore size and morphology can be controlled, by a spray-drying method using polystyrene latex (PSL) and silica colloids as the source materials. The pores sizes can be controlled using colloidal particles of different sizes. This is very easy because a huge variety of PSL and silica colloids of various particle sizes are currently commercially available. The porosity of the powders was investigated by scanning electron microscopy (SEM), transmission electron microscopy (TEM), and heat treatment. A high-temperature treatment removed the pores in the powder, giving solid particles. The difference in powder particle volume before and after annealing determines the porosity of the powder.

Mesoporous particles, obtained at equilibrium conditions using the procedure described above, have a specific and very regular structure. The pores are uniformly distributed on the surface of the sphere, in a hexagonal-like pattern. Questions of how such structures are produced, how the pattern of distribution occurs, and the kinetics of formation of mesoporous nanostructured particles by the spray-drying technique constitute the goal of this study.

Cell Structure on the Plane

The structure of matter, on both an atomic and macroscopic scale, is the result of the interplay between the requirements of the physical forces operating between the individual parts and the mathematical requirements of space filling. Unlike the underlying forces, the shapes of objects and their components are immediately apparent, and this explains why the observation and cataloguing of shapes is usually the first stage in development of any branch of science (see Thompson, 1942). It is the intent of this part of the paper to call attention to some elementary laws of topology and to use them to explain the process by which mesoporous particles are formed. Consider first the cell structure on the plane R^2. We assume that the cells are structuralized by "cell centers"—the distinguishing points in the cells—that are reference points for cell interactions.

Let $P = \{p_1, \ldots, p_N\}$ denote the set of points that represent the cell centers on the plane R^2. By $d_k(x) = d(x, p_k)$ we define the Euclidean distance function from p_k. The cell competition and the intercellular boundaries are defined by the gradient geometry of the global distance function.

Competitive range functions

To each cell $\hat{P}_k$, or to its organizing center p_k, we prescribe a cell-structure function $f_k\colon R^2 \to R$, $f_k > 0$. The global competition squared distance function is defined as follows:

$$\hat{d}(x) = \min\{f_1(x)d_1^2(x), \ldots, f_N(x)d_N^2(x)\} \tag{1}$$

The level curves of $\hat{d}$ can be considered as a type of wave front, which starts from points of the cell system P (Figure 1). The singularities of min or max of a finite number of smooth functions were previously examined (see, for example, Aurenhammer, 1991).

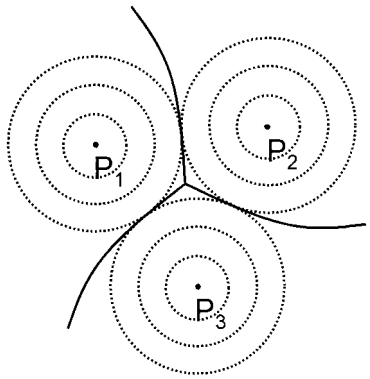

Figure 1. Organizing centers on the plane IR^2.

The cases of constant functions $f_i = const.$ are called Johnson–Mehl models. The function $\hat{d}$ is not differentiable exactly along the distinguished set (curve on the plane), also called the conflict set (see Siersma, 1999).

Conflict set arrangements and intercell patterns

The cells corresponding to the system of competition organizing centers $P_i = (p_i, f_i)$:

$$P = \{(p_1, f_1), \ldots, (p_N, f_N)\} \tag{2}$$

(where the points p_i are replaced by pairs P_i as structuralized centers), are defined as follows:

$$CP_i = \{x \in R^2 : \forall_{k \in \{1,\ldots,N\}} f_i(x)d_i^2(x) \le f_k(x)d_k^2(x)\} \tag{3}$$

An interface curve or generalized Voronoi diagram is defined as (see Aurenhammer, 1991)

$$VP = \{x \in R^2 : \exists_{i \neq j} s.that \forall_i f_i d^2(x, p_i) = f_j d^2(x, p_i) = f_j d^2(x, p_j) \le f_k d^2(x, p_k)\} \tag{4}$$

Further on, we consider the case $f_i \equiv 1$, $i = 1, \ldots, N$, and then the properties of the system P (the cell structure as well their boundaries) are the same as the distance function that has already been considered in Aurenhammer (1991), as illustrated in Figure 2.

The closed cell organized by P_i is defined as

$$V(P_i) = \{x \in R^2 : \forall_k d(x, p_i) \le d(x, p_k)\} \tag{5}$$

The function $\hat{d}$ is differentiable on the interior of all cells. A point set, where $\hat{d}$ is not differentiable, represents the curve of the intercells. At points of P the function $\hat{d}$ has its minimal value. The corresponding cell configurations are generically of two types, as shown in Figure 3. The saddle-minimum graph of $\hat{d}$ defines the global arrangements of the cells. Its vertices are points of P (minima of $\hat{d}$) and the edges are the line segments $p_i p_j$, which intersect the intercell edges $V(p_i) \cap V(p_j)$ in their interior (saddles of $\hat{d}$). The Euler formula for these graphs reads

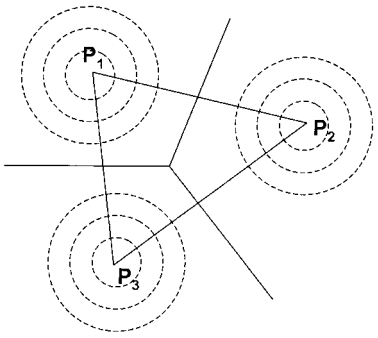

Figure 2. Voronoi diagram.

Cell structures and their boundaries.

$$V - E + R = 1 \qquad \text{(for the plane)} \tag{6}$$

where V is the number of vertices or minima of $\hat{d}$, E is the number of edges or saddles of $\hat{d}$, and R is the number of bounded regions defined by the graph, that is, the number of maxima of $\hat{d}$ (see examples in Figure 4).

Stationary Patterns of Centered Cell Arrangements on the Sphere

The spray-drying process used for the production of mesoporous nanostructured particles is described in detail in the experimental section. Colloidal mixtures of silica nanoparticles (sol type) and PSL nanoparticles were sprayed as droplets into a vertical reactor, which contains five temperature zones. Silica and PSL particles are more or less uniformly distributed within the spherical droplets. The PSL particles at the very beginning of the process are distributed on its surface, as the result of buoyancy forces. If the process permits the PSL particles to become organized on the sphere at the equilibrium configuration, rather than by the surface tension and interaction forces, the regular pattern of distribution of PSL particles results, with silica particles filling the space between them.

The solvent in the multiphase droplets evaporates in the lower zones of the reactor, producing a powder composite consisting of silica and PSL nanoparticles. The PSL nanoparticles in the powder decompose in the high-temperature zone, producing a silica powder consisting of mesopores. The question arises as to what the final structure of the mesoporous particles would be at equilibrium and how the process parameters affect the kinetics of reaching the equilibrium state.

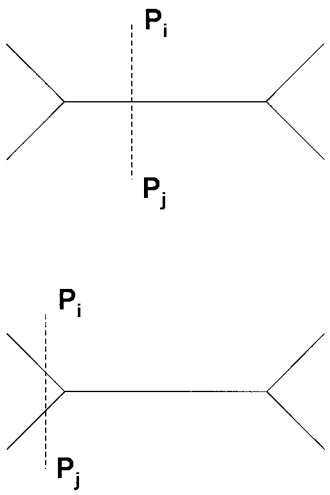

Figure 3. Saddle-minimum graph of the squared distance function.

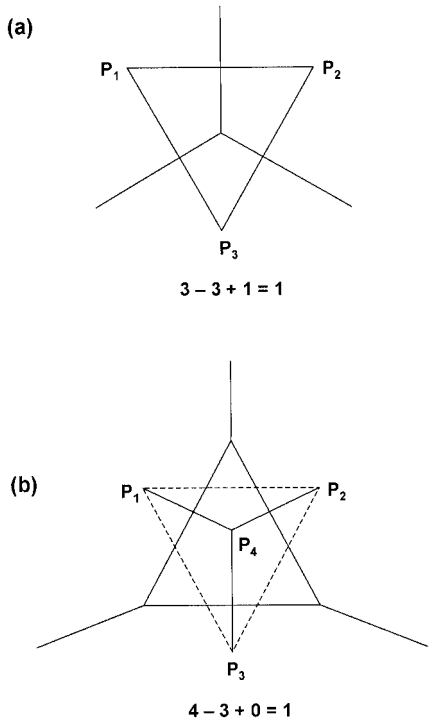

Figure 4. Examples of the Euler formula.

Equilibrium of interacting centers through the coexistence of cells on the sphere

The corresponding saddle-minimum graph of $\hat{d}$ defined on the sphere, describes the arrangement of cells on the sphere. The Euler formula in this case is obviously expressed as $V - E + R = 2$, where we redefine appropriate notions on the sphere endowed with an induced metric. An equilibrium arrangement of cells is organized by interactions through their boundaries around vortices that are combined globally into a

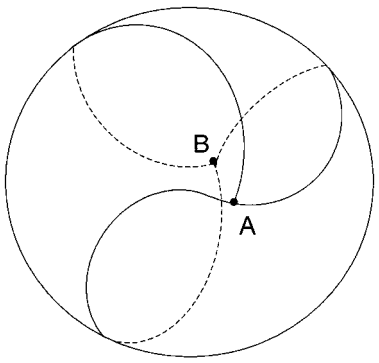

Figure 5. Two interacting particles A and B on the sphere.

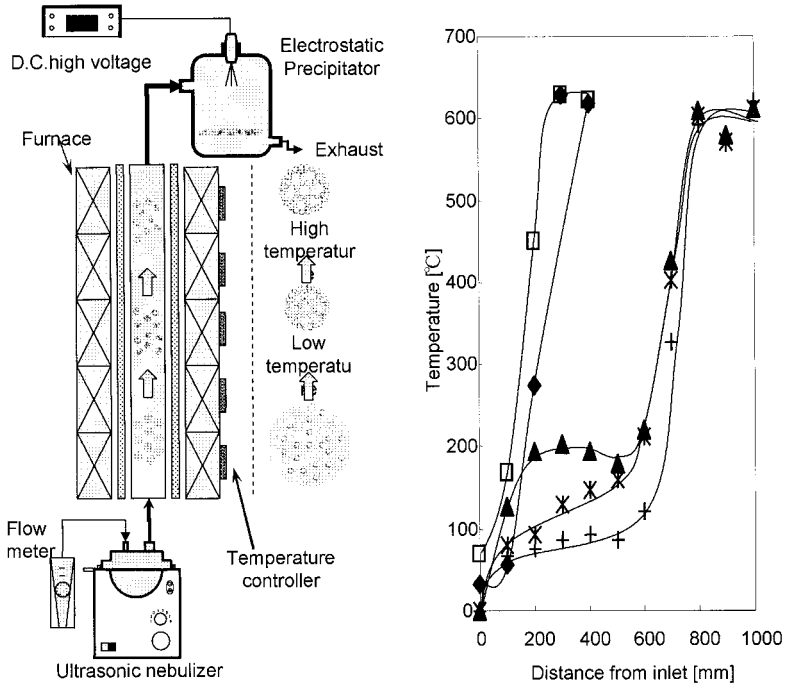

Figure 6. Left: experimental setup for the production of mesoporous particles; right: measured temperature inside the tube when the setting temperatures for the five zones (from bottom) are: (+) 100/100/100/600/600°C, (*) 100/150/200/600/600°C, (▲) 200/200/200/600/600°C, (◆) 25/600°C, and (□) 200/600°C.

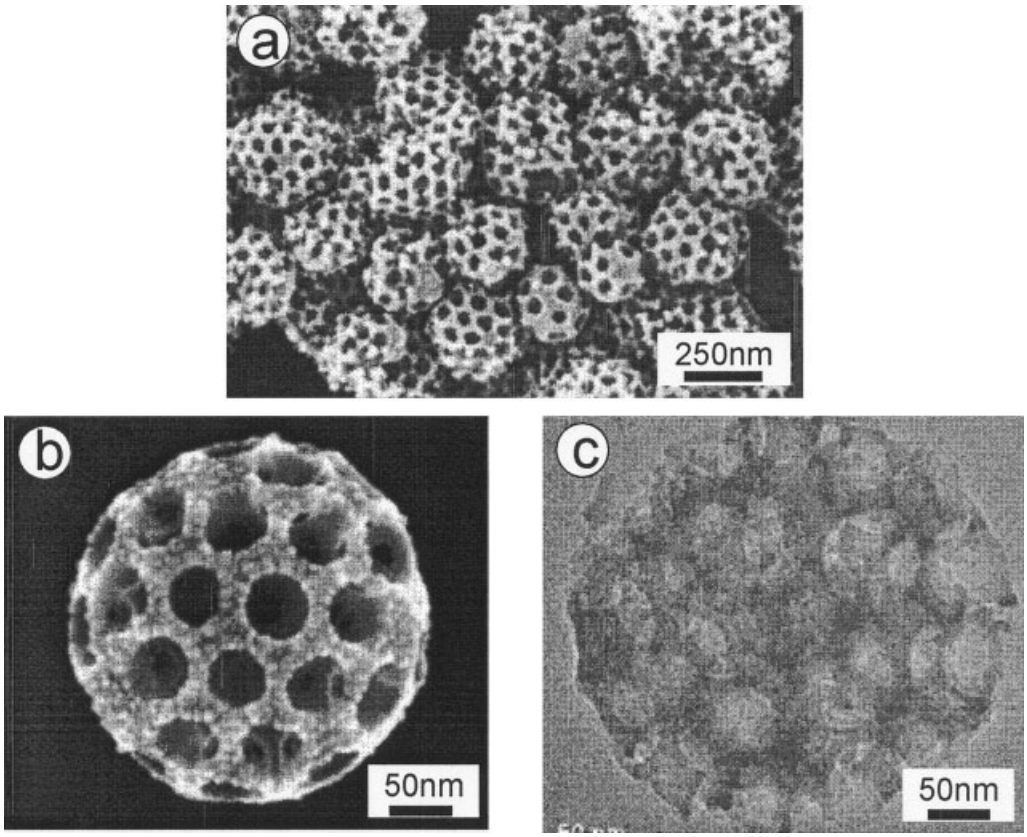

Figure 7. (a) SEM microphotographs of mesoporous particles obtained at stationary conditions (reference state); (b) enlarged view of a SEM micrograph of one selected particle; (c) TEM micrograph of one selected particle.

Synthesis parameters: SiO_2 (D_p = 5 nm, 0.025 wt %), PSL (D_p = 100 nm, 1 wt %), T: 100/150/200/600/600°C, and Q = 1 L/min.

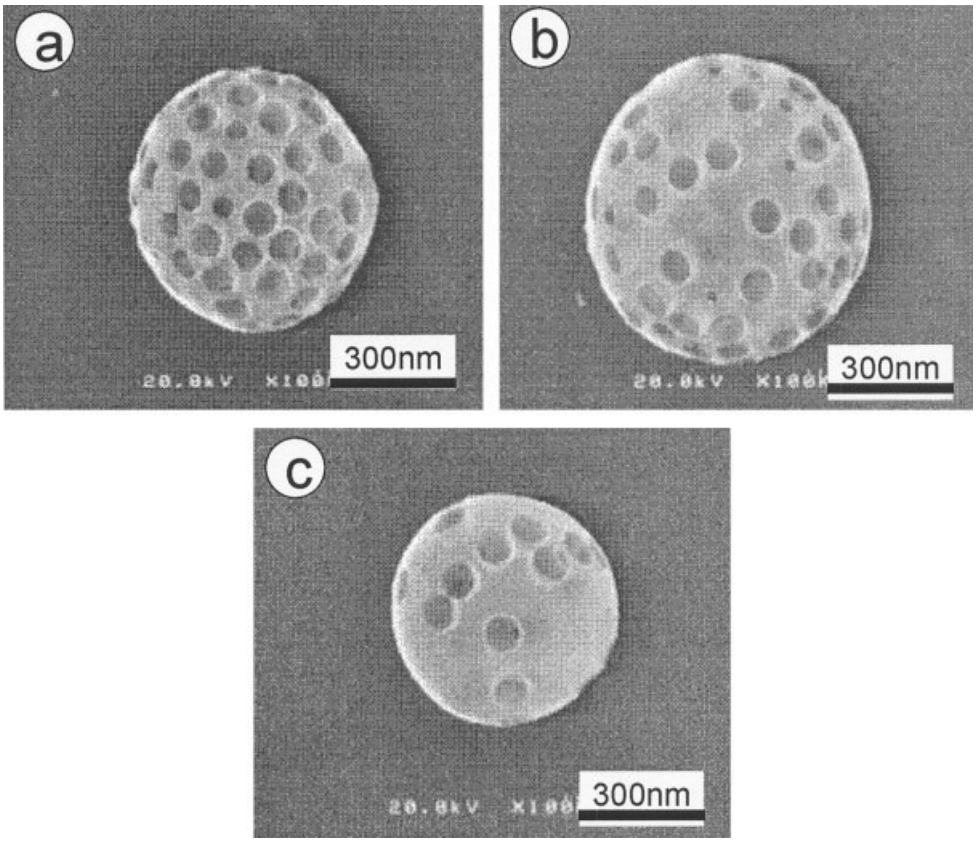

Figure 8. Particles obtained using a reduced concentration of PSL particles.

(a) 1 wt %, (b) 0.5 wt %, and (c) 0.25 wt %. Other synthesis parameters are SiO_2 (D_p = 5 nm, 0.025 wt %), PSL (D_p = 100 nm), T: 100/150/200/600/600°C, and Q = 1 L/min.

stabilized pattern. In the Appendix we propose a geometrical approach to the equilibrium of cells based on symplectic geometry methods (see Guillemin, 1984). As a straightforward result we find that the stationary state of the cell configuration on the sphere in the first approximation has equal infinitesimal angles of the cell boundaries in each vortex and they are equal to $2\pi/3$. Thus for a sufficient density of cells we obtain an almost hexagonal pattern of the identically competitive centers results (see also Luminet, 2003).

Obviously a sphere cannot be globally filled with hexagonal patterns. However, for a sufficiently large density, the other completing cells are exceptional. Surprisingly, an equal-angle principle in triple vortices and natural sphere geodesics as Voronoi edges critically restricts the number of possible equilibrium nets to the well-known ten types (see, for example, Heppes, 1964). The small number of cells in that distinct pattern does not exceed 12 (vortices in the saddle-minimum graph). This case is built by 30 arcs forming a single skeleton of a regular spherical dodecahedron. The case of ten cells in equilibrium is given by 24 arcs forming two regular quadrilaterals and eight equal pentagons, where each quadrilateral is surrounded by four pentagons and each pentagon is surrounded by four pentagons and one quadrilateral.

If cell centers are assumed to be interacting particles and the corresponding conflict set (intercell boundary) for the equilibrium system, then the 120° role in vortices is no longer globally true. Asymptotically, However, a majority of vortices fulfill this role (see Appendix and simplified approach there) and an almost regular hexagonal structure of cells is obtained as in the planar self-organization phenomenon commonly observed in nature (see, for example, Buzano, 1983).

Two interacting particles, cell centers, on the sphere are positioned on the antipodal points, Figure 5. The three particles form a regular triangle. Four centers form a regular tetrahedron. Five particles (and so on) are placed in regular configurations that minimize the total distance function. The stable configuration of centers on the sphere is determined by the corresponding generic cell boundary pattern, that is, the generic Voronoi diagram. A detailed analysis of this problem will form the basis of future studies.

Kinetics of the ordering process

As mentioned above, the ordering process consists of two terms; in the first, the fast stage, PSL particles move radially from the inner part of the droplet toward its surface because of buoyancy forces, and the surface of droplet then begins a second, slower step, driven by surface tension. In previous sections of this work we indicated that, at equilibrium, the cells are centered by the positions of PSL particles forming a hexagonal structure. At this moment, we propose the use of simple kinetics of ordering and organization for the cells, which minimize weak interactions of all cells on the sphere through minimization of the sum of the "perimeters" of all the cells on

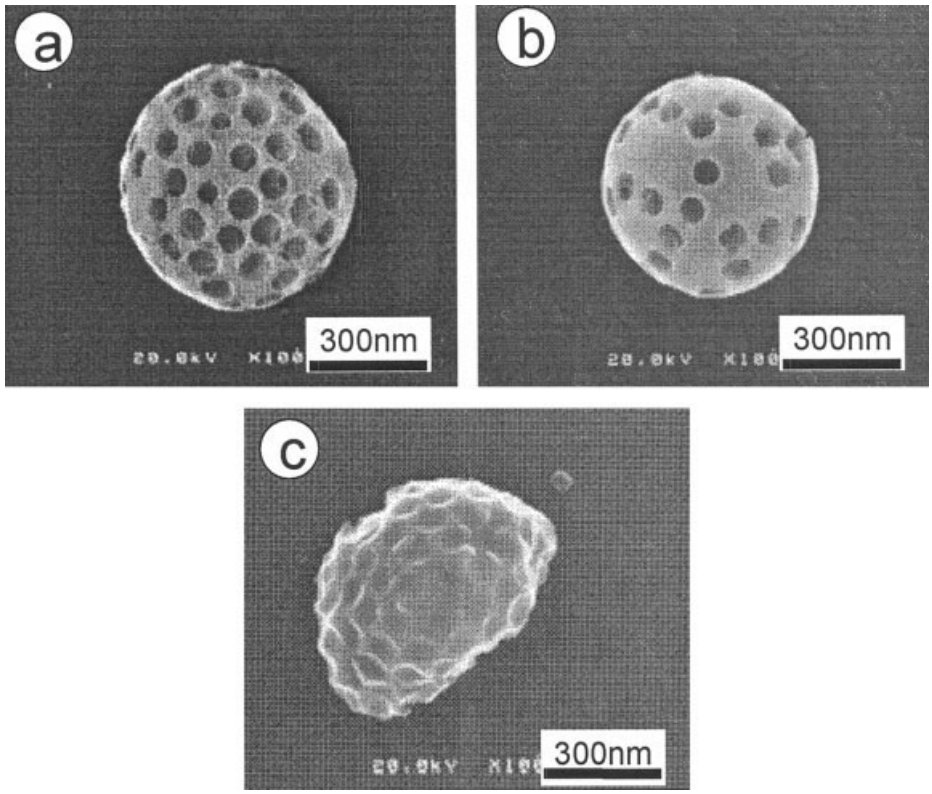

Figure 9. Effect of residence time on particle structure, controlled by gas flow rates.

(a) 1 L/min, (b) 2 L/min, and (c) 5 L/min. Other synthesis parameters are SiO_2 (D_p = 5 nm, 0.025 wt %), PSL (D_p = 100 nm, 1 wt %), T: 100/150/200/600/600°C.

the surface, N. This reaches a minimum when the angles at the vertex of the cell are the same and equal to $2\pi/3$. At the beginning, after a very short interval dt, PSL particles are randomly distributed on the surface of the droplet. Cells that are centered by PSL particles have random shapes. Surface tension, which minimizes surface energy, causes the restructurization of the cells (by mitosis, rearrangement, and vanishing). Silica particles follow this process and their displacement rate is determined by particle diameter. The kinetic equation describing the organization of the cells has the form

$$\frac{dN}{dt} = K(\sigma, D)N(\alpha, \beta, \gamma) - N\left(\frac{2\pi}{3}, \frac{2\pi}{3}, \frac{2\pi}{3}\right) \qquad (7)$$

The kinetics coefficient K denotes the function of the surface tension σ at the interface carrier gas droplets, which is a driving force in the process of ordering, and the mobility D of the silica particles at the interface when the space between the moving PSL particle is filled.

In the experimental part of our work, we attempted to

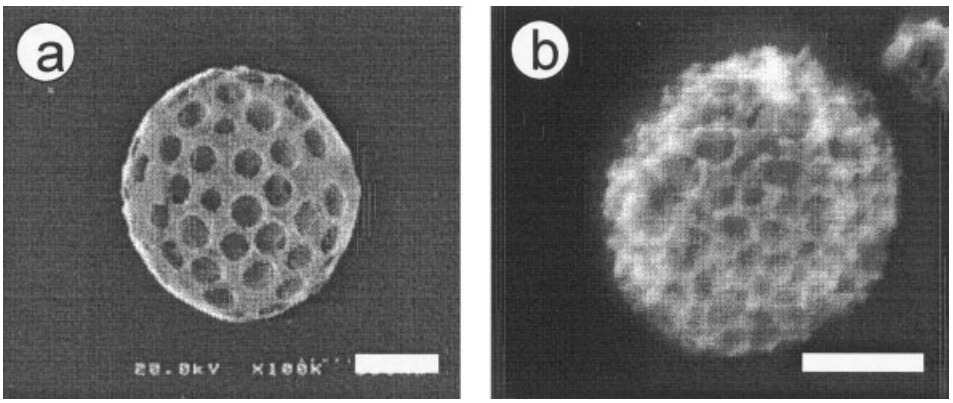

Figure 10. Effect of residence time on particle structure, controlled by the length of the drying zone.

(a) 1.0 m, T: 100/150/200/600/600°C and (b) 0.2 m, T: 200/600°C. Other synthesis parameters are SiO_2 (D_p = 5 nm, 0.025 wt %), PSL (D_p = 100 nm, 1 wt %), and Q = 1 L/min. Bar scale: 200 nm.

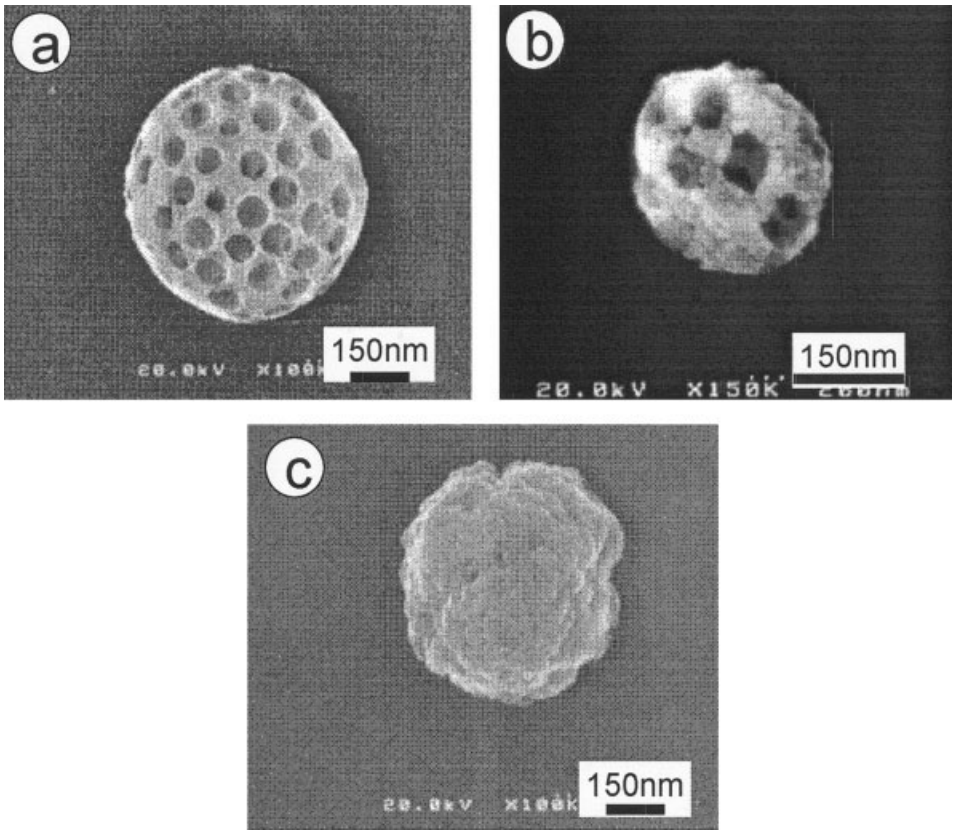

Figure 11. Influence of surface tension on the ordering process.

The surface tension was controlled by adding surfactant in various concentrations: (a) 0 wt %, (b) 0.1 wt %, and (c) 0.5 wt %. Other synthesis parameters are SiO_2 (D_p = 5 nm, 0.025 wt %), PSL (D_p = 100 nm, 1 wt %), T: 100/150/200/600/600°C, and Q = 1 L/min.

prove the hypothetical explanation of the kinetics of ordering of mesopores at the surface, before the hexagonal structure of the pattern is reached. As mentioned above, the set of parameters that determine the kinetics of the formation of mesopores includes the material properties of the system: the silica particle size (determining their displacement rates at the surface), the surface tension of the liquid forming a droplet, and the operational conditions used in the process, that is, the structure of heating along droplet displacement and the flow rates of the droplets through the reactor, which determine residence time.

Experimental

Figure 6 (left) shows the experimental setup used to prepare the mesoporous nanostructured silica particles from colloidal suspensions. The setup is similar to that used in our previous studies (see Iskandar et al., 2001a–c, 2002, 2003c,d). It consists of three sections: (1) a spray generator, (2) a vertical tubular furnace, and (3) a particle collector. Colloidal suspensions of nanosized silica and polystyrene latex (PSL) were used as the precursors for producing submicron-sized silica particles in a mesoporous state. The spray generator used was an ultrasonic spray nebulizer, equipped with a 1.75-MHz resonator (Omron Corp., Ibaraki, Japan). The atomized droplet size (from water as the precursor), as measured by a light-scattering particle size analyzer (Malvern Instruments Corp., Worcestershire, U.K.), was in a range between 1 and 11 μm, and the mean particle size was about 4.5 μm. The droplets were carried into a tubular reactor by a stream of nitrogen gas. The flow rates were varied in the range of 1 to 5 L/min. The reactor size was 0.013 m in inner diameter and 1.0 m in length, divided into five arbitrary temperature-controllable zones (each 0.2 m in length). Figure 6 (right) shows the measured temperature inside the tube at various setting temperatures: (+) 100/100/100/600/600°C, (*) 100/150/200/600/600°C, (▲) 200/200/200/600/600°C, (◆) 25/600°C, and (□) 200/600°C. The prepared particles were collected using a filter maintained at 150°C to prevent water condensation. Colloidal suspensions of silica (silica sol) were obtained from Nissan Chemical Industry Ltd. The nominal particle sizes, as measured by TEM were 5 ± 1, 15 ± 5, and 25 ± 5 nm. A PSL colloid containing 100-nm spherical particles was obtained from Japan Synthetic Rubber. The colloidal silica particles and colloidal PSL particles were diluted with water to give the expected concentration and then mixed in various weight fractions. To study the effect of surfactant, a droplet containing a surfactant at levels of 0.05, 0.08. 0.1, and 0.5 wt. % were mixed with the precursor before spraying. The morphology of the prepared particles was observed using a field emission scanning electron microscope (FE-SEM S-5000, Hitachi, Osaka, Japan) and a transmission electron microscope (HR-TEM 2200, Hitachi).

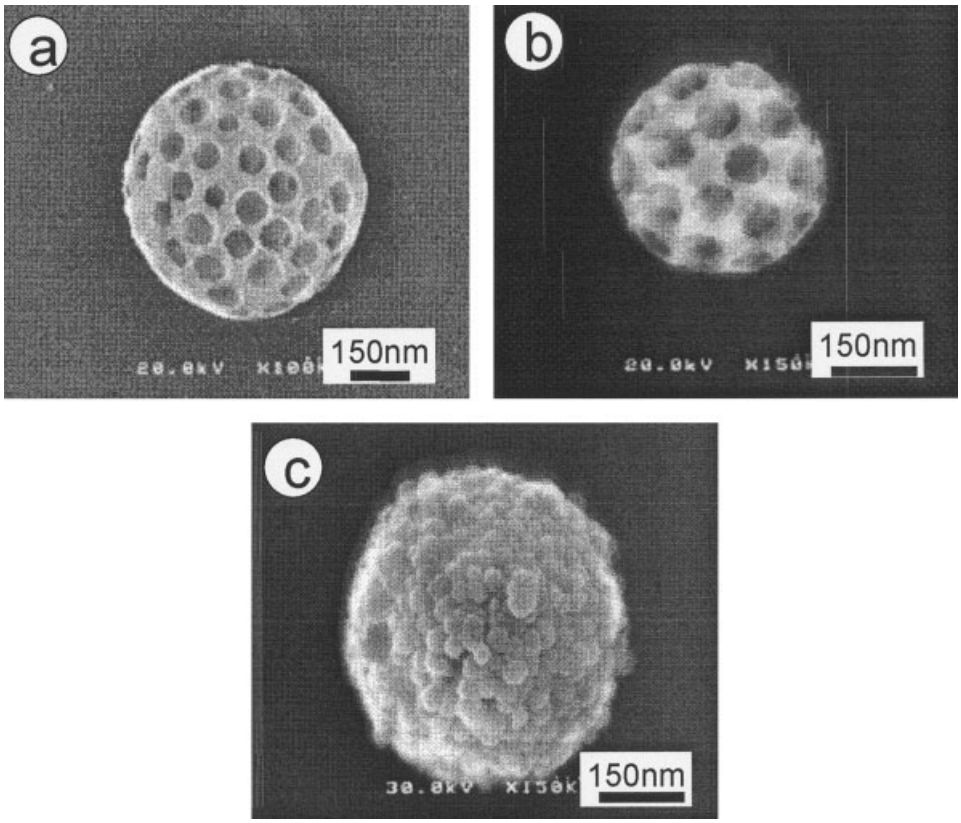

Figure 12. Particles obtained using different diameters of silica particles.

(a) 5 nm, (b) 15 nm, and (c) 25 nm. Other synthesis parameters are SiO_2 (0.025 wt %), PSL (D_p = 100 nm, 1 wt. %), T: 100/150/200/600/600°C, and Q = 1 L/min. Bar scale: 200 nm.

Results and Discussion

Figure 7 shows SEM and TEM microphotographs of the ordered mesoporous particles. The particles were made using SiO_2 (D_p = 5 nm, 0.025 wt %), PSL (D_p = 100 nm, 1 wt. %), T: 100/150/200/600/600°C, and Q = 1 L/min. Using these parameters the synthesis of mesoporous nanostructured particles with a hexagonal patterns were obtained. A variety of synthesis parameters were examined and the above parameters were found to result in particles having the best morphology (porous organization). We refer to the above parameters as the reference state. Based on TEM micrographs, pores were also found inside the particle.

Changing this reference state perturbs the nature of the particles produced by process. As mentioned above, the ordering of PSL particles at the surface of a droplet depends on the initial number of these particles in the droplet. We changed the concentration of PSL particles in the primary suspension, reducing it to the values C = 0.5 wt % and C = 0.25 wt. %. The other parameters were similar to those used to produce the particles shown in Figure 7. One can see in Figure 8 that a hexagonal pattern does not result when the number of PSL particles is below a certain value, which defines the complete filling of the space. When the silica particle fraction was very high, a type of silica-coated porous particles was obtained.

The primary parameter, which influences the kinetics of ordering, is the residence time of the droplet in the evaporation (low-temperature) zone of the system. This can be checked by changing the flow rates of the droplet through a reactor with a defined temperature distribution, or by changing of the lengths of evaporation zones. Figure 9 shows the effect of flow rate on particle morphology. Three flow rates were used: Q = 1, 2, and 5 L/min, corresponding to residence times of 1.5, 0.75, and 0.3 s, respectively. The other parameters were SiO_2 (D_p = 5 nm, 0.025 wt. %), PSL (D_p = 100 nm, 1 wt. %), and T: 100/150/200/600/600°C. An increase in flow rate causes the deformation of droplets as a result of the high drag forces that act on them. The final particle has a deformed shape for flow rates higher than 1 L/min.

When the residence time is decreased by reducing the length of the evaporation zones at a low flow rate (Q = 1 L/min), spherical mesoporous particles are obtained but the mesopores are positioned irregularly, with some effects of agglomeration of PSL particles (Figure 10). The residence time was too short to permit an ordering process. A similar conclusion was reached for the organization of PSL beads from a droplet containing PSL particles (see, for example, Mikrajuddin et al., 2002).

The driving force for ordering particles is surface tension. In the case of the reference state, the surface tension was changed by adding a surfactant to the water at concentrations of 0.1 and 0.5%. The synthesis parameters were SiO_2 (D_p = 5 nm, 0.025 wt. %), PSL (D_p = 100 nm, 1 wt. %), T: 100/150/200/600/600°C. Particles produced under these conditions are shown in Figure 11. The pores on particle surfaces were irregular. PSL

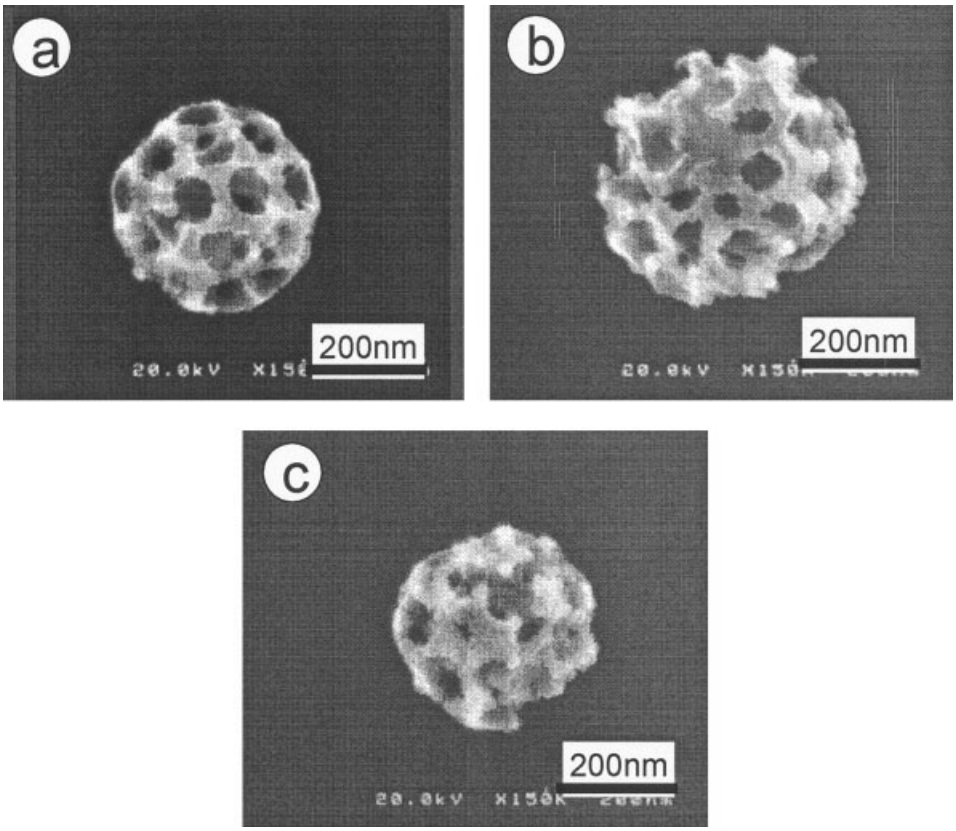

Figure 13. Particles obtained for the simultaneous decreasing of surface tension and increasing of silica particle diameter.

Concentrations of surfactants are: (a) 0 wt. %, (b) 0.05 wt. %, and (c) 0.08 wt. %. Other synthesis parameters are SiO_2 (D_p = 15 nm, 0.025 wt. %), PSL (D_p = 100 nm), T: 100/150/200/600/600°C, and Q = 1 L/min.

particles were not distributed uniformly. Agglomerates of these particles left pores in different sizes and shapes.

At the final stage of our experimental investigations, the diameters of silica particles were changed. Larger particles with a larger mass have lower mobility. The displacement rate of these particles is smaller than that for larger particles. Silica particles with diameters of 15 and 25 nm were used in this experiment, in addition to the 5 nm particles used at the reference state. Figure 12 shows that irregular or no mesopores are present when larger SiO_2 particles are used at the experimental condition defined for the reference state.

In addition to these specific experiments we simultaneously changed the surface tension and silica particle size in the final experiment. The results, shown in Figure 13, indicate the influence of both parameters—surface tension and particle mobility—that is, the value of the self-organization process in the formation of the mesoporous particles.

Conclusions

Mesoporous nanostructured silica particles with a controllable porous size were produced by a spray-drying method. The mesopores were arranged into a hexagonal packing state, indicating that a self-organization process spontaneously occurred during solvent evaporation. The stationary pattern of the centered cell arrangements on the surface of a sphere has a hexagonal form if the amount of PSL particles used in the process is sufficient to cover the surface of the sphere with the highest packing density. The use of Voronoi diagrams in the model proved that the stationary state of the cell configuration on the sphere has infinitesimal angles of cell boundaries in each vortex and are equal to $2\pi/3$ (that is, the cell structure has a hexagonal form). The proposed kinetics of the self-organization process shows that the driving force for ordering is the surface tension and surface mobility of the silica particles. Examples of particles produced at nonstationary conditions indicate the influence of process parameters on the kinetics of ordering of mesopores.

Notation

P = organizing centers on a sphere
d = Euclidean distance function
f = cell-structure function
V = number of vertices
E = number of edges
R = number of bounded regions
N = length of the cell perimeters
D = surface mobility of silica particles
σ = surface tension
K = kinetics coefficient

Literature Cited

Aurenhammer, F., "Voronoi Diagrams—A Survey of a Fundamental Geometric Data Structure," *ACM Comput. Surveys*, **23**, 345 (1991).

Buzano, E., and M. Golubitsky, "Bifurcation on the hexagonal lattice and the planar Benard problem," *Philos. Trans. R. Soc. Lond. A*, **308**, 617 (1983).
Guillemin, V. W., and S. Sternberg, "Symplectic Techniques in Physics," Cambridge Univ. Press, Cambridge, U.K. (1984).
Heppes, A., "Isogonal spharischen netze," *Ann. Univ. Sci. Budapest Eotvos Sect. Math.*, **7**, 41 (1964).
Huo, Q., J. Feng, F. Schuth, and G. D. Stucky, "Preparation of Hard Mesoporous Silica Spheres," *Chem. Mater.*, **9**, 14 (1997).
Iskandar, F., M. Abdullah, H. Yoden, and K. Okuyama, "Optical Band Gap and Ultra Low Dielectric Constant Materials Prepared by a Simple Dip Coating Process," *J. Appl. Phys.*, **93**, 9237 (2003a).
Iskandar, F., M. Abdullah, H. Yoden, and K. Okuyama, "Ordered Porous Silica Films Prepared by Simple Dip Coating of Silica Nanoparticles and Polystyrene Beads Colloids and the Application as Reflection-Mode Monochromator," *J. Sol-Gel Sci. Technol.*, in press (2003b).
Iskandar, F., H. Chang, and K. Okuyama, "Preparation of Microencapsulated Powders by an Aerosol Spray Method and Their Optical Properties," *Adv. Powder Technol.*, **14**, 349 (2003c).
Iskandar, F., L. Gradon, and K. Okuyama, "Control of the Morphology of Nanostructured Particles Prepared by the Spray Drying of a Nanoparticle Sol," *J. Colloid Interface Sci.*, **265**, 296 (2003d).
Iskandar, F., I. W. Lenggoro, T.-O. Kim, N. Nakao, M. Shimada, and K. Okuyama, "Fabrication and Characterization of SiO_2 Particles Generated by Spray Methods for Standards Aerosol," *J. Chem. Eng. Jpn.*, **34**, 1285 (2001b).
Iskandar, F., I. W. Lenggoro, B. Xia, and K. Okuyama, "Functional Nanostructured Silica Powders Derived from Colloidal Suspensions by Sol Spraying," *J. Nanoparticle Res.*, **3**, 263 (2001c).
Iskandar, F., Mikrajuddin, and K. Okuyama, "In Situ Production of Spherical Silica Particles Containing Self-Organized Mesopores," *Nano Lett.*, **1**, 231 (2001a).
Iskandar, F., Mikrajuddin, and K. Okuyama, "Controllability of Pore Size and Porosity of Self-Organized Porous Silica Particles," *Nano Lett.*, **2**, 389 (2002).
Janeczko, S., "Lagrangian Submanifolds in Product Symplectic Spaces," *J. Math. Phys.*, **41**, 5642 (2000).
Luminet, J.-P., J. R. Weeks, A. Riazuelo, R. Lehoucq, and J.-P. Uzan, "Dodecahedral Space Toplogy as an Explanation for Weak Wide-Angle Temperature Correlations in the Cosmic Microwave Background," *Nature*, **425**, 593 (2003).
Marsden, J. E., *Lectures on Mechanics*, London Mathematical Society Lecture Note Series 174, Cambridge Univ. Press, Cambridge, U.K. (1992).
Mikrajuddin, F. Iskandar, and K. Okuyama, "Single Route for Producing Organized Metallic Domes, Dots, and Pores by Colloidal Templating and Over Sputtering," *Adv. Mater.*, 14, 930 (2002).
Ozin, G., "Nanochemistry: Synthesis in Diminishing Dimensions," *Adv. Mater.,* **4**, 612 (1992).
Park, S. H., D. Qin, and Y. Xia, "Crystallization of Meso-Scale Particles over Large Areas," *Adv. Mater.*, **10**, 1028 (1998).
Siersma, D., "Properties of conflict sets in the plane," *Geometry and Topology of Caustics'98, Banach Center Publications*, **50**, 267 (1999).
Thompson, D. W., *On Growth and Form*, Cambridge Univ. Press, Cambridge, UK (1942).
Velev, O. D., T. A. Jede, R. F. Lobo, and A. M. Lemhoff, "Microstructured Porous Silica Via Colloidal Crystallization," *Nature*, **389**, 447 (1997).
Velev, O. D., and E. W. Kaler, "Structured Porous Materials via Colloidal Crystal Templating: From Inorganic Oxides to Metals," *Adv. Mater.*, **12**, 531 (2000).
Zakhidov, A. A., R. H. Baughman, Z. Iqbal, and C. X. Cui, "Carbon Structures with Three-Dimensional Periodicity at Optical Wavelengths," *Science*, **282**, 897 (1998).

Appendix: Phase Space for Configuration of Equilibrium Cells

Let us introduce a notion of the phase space based on the canonical symplectic approach to natural phenomena (see Guillemin et al., 1984). Let P denote the configurational space of a given cell. Usually this is a range of positions of the organizing centers of a cell (including constraints and nontrivial topology).

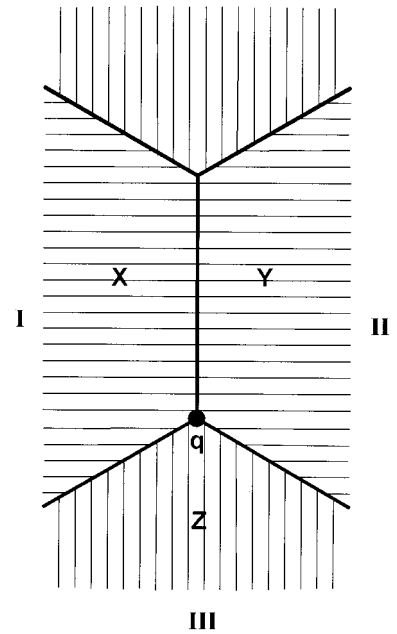

Figure A1. Cells prescribed to the vortex q on the sphere.

To the elements of P we prescribe the natural polar coordinates—"forces"—responsible for the directional dynamics of a center. The space, defined in this manner corresponds, mathematically, to the cotangent bundle of P, denoted by T^*P [conjugate at each point of P to the tangent space TP (see Marsden, 1992)]. Infinitesimal elements allowing integration of the action of forces f_i on displacements of configurations p_i define a differential form of energy, which corresponds to the classical Liouville form on a cotangent bundle, say

$$\theta_P = \sum f_i dp_i$$

in local coordinates. The equilibrium states of the system are realized on a subset (submanifold), say L, of T^*P, defined by the constitutive equations and having crucial isotropicity properties, that is, the differential of the Liouville energy form $d\theta_P$ is vanishing on L: $d\theta_P|_L = 0$. Such submanifolds are called Lagrangian and are generated (always locally) by functions, called generating functions, having the sense of potentials, Hamiltonians, and so forth.

Now for the system of interacting cells we generalize on this notion.

To each vortex q of the intercells graph we prescribe three cells that interact through their competitive centers (Figure A1). If X, Y, and Z are the configurational spaces of cells I, II, and III, respectively (X, Y, and Z spaces may parameterize the center positions around the vortices nearest the configuration cells), then we define the intercell interaction phase space (between two neighboring cells, such as I and II), which is the product symplectic space (see Janeczko, 2000)

$$(T^*X \leftrightarrow T^*Y,\ d\theta_Y - d\theta_X) \tag{A1}$$

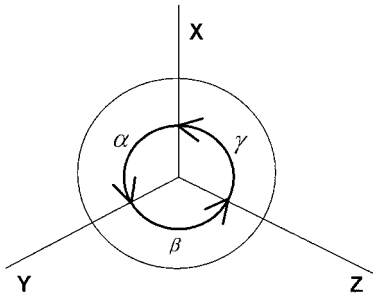

Figure A2. Structure of the nearest neighboring cells.

where T^*X and T^*Y are the cotangent bundles, that is, phase spaces for the corresponding cells; $d\theta_Y$ and $d\theta_X$ are their Liouville forms, $d\theta_Y - d\theta_X = \pi_Y{}^* d\theta_Y - \pi_X{}^* d\theta_X$; and π_X, π_Y are canonical projections of the Cartesian product $T^*X \times T^*Y$.

Equilibrium configurations of two interacting cells remain in a submanifold $L \subset T^*X \leftrightarrow T^*Y$, which is Lagrangian, that is, $d\theta_Y - d\theta_X|_L = 0$. A generating function F corresponding to L, $F : X \leftrightarrow Y \to R$, reflects the collective interaction potential of the cells. To each vortex q we associate the nearest neighboring cells. In a generic position, we have only the triple vortices, as schematically shown in Figure A2.

In homogeneously distributed interactions of cells that have identical configurational spaces, we have $X \cong Y \cong Z$. The stable configuration of cells in a given vortex is a closed orbit of L, that is

$$\{x, y = L(x), z = L \circ L(x), L \circ L \circ L(x) = x\} \quad \text{(A2)}$$

If x, y, and z denote the polar coordinates of the cell's centers on a circle, then the closed triple orbit of L is defined as a critical point of the symplectically invariant function (see Janeczko, 2000)

$$\tilde{F}(x, y, z) = F(x, y) + F(y, z) + F(z, x) \quad \text{(A3)}$$

Furthermore, we obtain the corresponding equations for equilibrium

$$\frac{\partial F}{\partial u}(x, y) + \frac{\partial F}{\partial v}(z, x) = 0 \qquad \frac{\partial F}{\partial u}(y, z) + \frac{\partial F}{\partial v}(x, y) = 0$$

$$\frac{\partial fF}{\partial u}(z, x) + \frac{\partial F}{\partial v}(y, z) = 0 \quad \text{(A4)}$$

where, by u and v denote the arguments of function F.

We assume that the potential interaction function F depends on the angular distances of the centers, that is, $F(x, y) = G(x - y)$, where G is a smooth monotonous function. Then the Eq. A4 system gives

$$\frac{\partial G}{\partial w}(x - y) - \frac{\partial G}{\partial w}(z - x) = 0$$

$$\frac{\partial G}{\partial w}(y - z) - \frac{\partial G}{\partial w}(x - y) = 0,$$

$$\frac{\partial G}{\partial w}(z - x) - \frac{\partial G}{\partial w}(y - z) = 0 \quad \text{(A5)}$$

and solving them we obtain

$$\alpha = (x - y) = (z - x) > 0$$

$$\beta = (y - z) = (x - y) > 0$$

$$\gamma = (z - x) = (y - z) > 0 \quad \text{(A6)}$$

where x, y, and z are angular oriented coordinates counted modulo 2π, $(z - x) + (x - y) + (y - z) = \alpha + \beta + \gamma = 2\pi$. From the preceding system of equations (Eq. A6) we have $\alpha = \beta = \gamma = 2\pi/3 = 120°$. Thus the following is obtained.

Corollary. *The stationary state of the cell configuration on the sphere in a first approximation has equal infinitesimal angles of cell boundaries in each vortex and this angle is equal to $2\pi/3$. Thus for a sufficient density of cells we obtain a nearly hexagonal pattern of identically competitive centers.*

Assuming that the potential functions F are identical for all intercell arcs and conjugating all vortices globally on the sphere by Eq. A4 we obtain the only ten possible types of cell arrangements on the sphere (see Heppes, 1964). However, there are obstacles to such a homogeneity and the equilibrium configurations of cells with equal interacting potentials do not exist for high numbers of cells. An asymptotic pattern dominated by hexagons can also be obtained in a simplified way (as suggested by a referee). In fact, if we assume that a Voronoi diagram has only threefold vortices and regular faces with n edges each, then one can immediately write the following relations: $nR = 2E$, $2E = 3V$. By the Euler characteristic formula $V - E + R = 2$, an equation involving n and E only is obtained, that is

$$(2/n - 1/3)E = 2$$

which has exact solutions only for $n = 3$, 4, and 5, and $n = 6$ in the limit case for E tending to infinity.

Obviously the sphere cannot be globally filled with hexagonal patterns. However, for a sufficiently large density, the other completing cells are necessarily expected, however exceptional.

Manuscript received Sep. 21, 2003, and revision received Jan. 14, 2004.